ISSN 1070-4272, Russian Journal of Applied Chemistry, 2020, Vol. 93, No. 12, pp. 1837–1844. © Pleiades Publishing, Ltd., 2020.
Russian Text © The Author(s), 2020, published in Zhurnal Prikladnoi Khimii, 2020, Vol. 93, No. 12, pp. 1740–1748.

INORGANIC SYNTHESIS
AND INDUSTRIAL INORGANIC CHEMISTRY

Synthesis and Electrochemical Research of the Properties of Mixed Nickel-Cobalt Oxides as Materials for Energy Storage Devices

A. I. Volkov[a], D. V. Zhuzhel'skii[a], E. G. Tolstopyatova[a], and V. V. Kondratiev[a,*]

[a] *St. Petersburg State University, St. Petersburg, 199034 Russia*
**e-mail: vkondratiev@mail.ru*

Received May 21, 2020; revised August 2, 2020; accepted August 10, 2020

Abstract—Mixed nickel-cobalt oxide was prepared by hydrothermal synthesis. The morphology and structure of the produced oxide were studied using scanning electron microscopy and X-ray structural analysis: spinel $NiCo_2O_4$ forms spherical nanostructures. Electrodes were prepared from composite materials based on nickel-cobalt mixed oxides, polyvinylidene fluoride binder, and carbon black, applied to nickel foam by various methods. Electrochemical studies of electrodes in aqueous alkaline solutions have been carried out by the cyclic voltammetry. The obtained values of the specific capacity of the material in charge-discharge cycling reach 840 F g^{-1} at 5 mV s^{-1}. The best value of the capacity retention of the produced materials is 87% for 100 cycles.

Keywords: mixed nickel-cobalt oxides, hydrothermal synthesis, morphology, specific capacity

DOI: 10.1134/S1070427220120058

In recent years, metal oxides were widely studied as possible materials for pseudocapacitors prepared based on fast redox transformations of metal ions in the bulk and on the surface of the electrode material [1, 2]. They are characterized by higher capacities than double-layer capacitor materials, however, at present they are noticeably inferior in the stability of electrochemical properties with multiple repetitions of the recharging process [3].

Among the promising materials of this group are mixed nickel-cobalt oxides as possible materials for use in various electrochemical applications: supercapacitors [4–7], batteries [8], catalysts [9, 10], etc. In recent years, studies of materials based on mixed nickel-cobalt oxides have become a fairly large area, comparable in importance with studies of long-known manganese oxide and ruthenium oxide [11]. Mixed nickel-cobalt oxides (and hydroxides) of various structures exhibit electrochemical activity mainly in alkaline solutions [12, 13]. One of their advantages as a compound of two types of metals over individual metal oxides of nickel or cobalt is an increased (by 2 orders of magnitude) electronic conductivity of the material [14, 15]. Nevertheless, composites with conductive additives, in particular, with carbon materials, are used to further improve the conductivity of the electrode material [16–18]. An important role is also played by the production of nanostructures of the material, which can make it possible to reduce the mechanical stress in the material due to the recharge processes [19].

The purpose of the work is to synthesize mixed nickel-cobalt oxide with its subsequent study as a component of electrode materials for energy storage devices. In the course of the study, the electrochemical properties of the mixed nickel-cobalt oxide as a component of a composite material with carbon black cast on nickel foam electrode substrate were studied. Electrochemical studies of the prepared electrodes were carried out by cyclic voltammetry in 2 M KOH solutions. The specific capacities of the material based on mixed oxide were determined.

EXPERIMENTAL

The following reagents were used in the work: cobalt nitrate hexahydrate (extra pure grade), nickel nitrate hexahydrate (pure grade), urea (pure grade) and potassium hydroxide (pure grade) (all

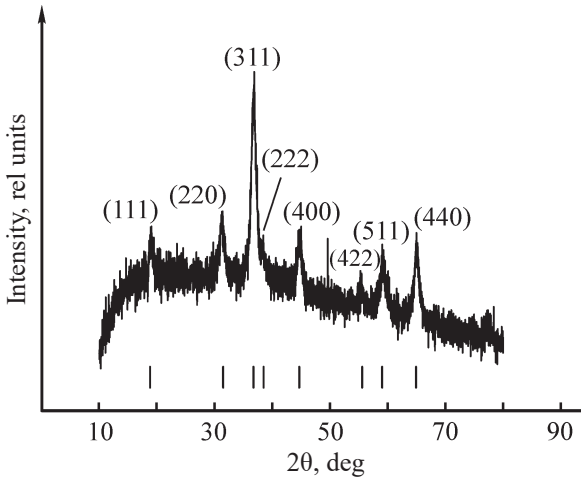

Fig. 1. X-ray diffraction pattern of the $NiCo_2O_4$powder.

produced by Reakhim), polyvinylidene fluoride and *N*-methylpyrrolidone (Sigma-Aldrich), Super P carbon black (Timcal Inc.), nickel foam (MTI Corp.) with a specific surface area of 350 $m^2 g^{-1}$.

For preparing solutions, deionized water was utilized, produced using a Millipore Direct-Q UV purification system (Millipore Corp.).

$NiCo_2O_4$ was synthesized hydrothermally; 10.5 mmol of cobalt nitrate, 4.5 mmol of nickel nitrate, and 15 mmol of urea were dissolved in 32 mL of water. The solution was transferred to 50 mL polypropylene-lined stainless-steel autoclave then the autoclave was kept at 130°C for 24 h. The pink precipitate was collected from the autoclave and washed several times with water, then it was dried and calcined at 300°C for 2 h.

Several types of electrodes were produced. To prepare the first type of electrodes, hereinafter denoted as NC_{NMP}, the resulting $NiCo_2O_4$ powder (80 wt %), carbon black (10 wt %), and polyvinylidene fluoride binder (10 wt %), dissolved in *N*-methylpyrrolidone, were thoroughly mixed in an agate mortar. The resulting electrode mixture was applied to the nickel foam with a brush until the 1 × 1 cm substrate area was uniformly covered. Then, the electrodes were dried for 5 h in a vacuum oven at 80°C. The dried electrodes were roll-pressed to a thickness of 50 μm. The mass loading of the active material $NiCo_2O_4$ (per 1 cm^2 of the visible surface of the substrate electrode) was 8 mg cm^{-2}.

The second type of electrodes, NC_{eth}, was prepared in a similar manner, but using ethanol as solvent. An evident advantage of ethanol over *N*-methylpyrrolidone was its good ability to penetrate into the pores of nickel foam. The mass loading of the active material in this case, was 5 mg cm^{-2}.

The third type of electrodes, NC_{foam}, was obtained by direct deposition of $NiCo_2O_4$ on the surface of nickel foam. During hydrothermal synthesis, nickel foam electrodes were placed in an autoclave together with a reaction solution. After synthesis, the nickel foam with a precipitate formed on it was calcined at 300°C for 2 h.

Electrochemical studies were carried out in a three electrode electrochemical cell at a temperature of 20 ± 2°C. The potentials were measured relative to a silver chloride reference electrode Ag/AgCl/$NaCl_{sat}$ (SCE, 0.197 V relative to SHE). A platinum coil (S = 5.0 cm^2) served as an auxiliary electrode. An Autolab PGSTAT 302N potentiostat (Metrohm Autolab) was used to carry out voltammetric measurements.

The morphology of the resulting deposits was studied using a Zeiss Supra 40VP scanning electron microscope.

X-ray diffraction analysis of the synthesized mixed oxide powder was conducted with a Bruker-AXS D8 DISCOVER high-resolution diffractometer with CuK_α radiation (λ = 0.15406 nm) in the 2θ range from 10° to 80°.

RESULTS AND DISCUSSION

The preparation of $NiCo_2O_4$ powder was confirmed by powder X-ray diffraction. The diffraction peaks of the spectrum (Fig. 1) correspond to the known data (ICDD N 01-073-1702) [20, 21]. The detected phase $NiCo_2O_4$ is characterized by the space group F*d*3*m*, which corresponds to a cubic crystal structure. According to Scherrer's equation, the size of individual crystallites is about 15 nm. The fact of such a small size indicated a high capacity of the material [21–23].

Images obtained using a scanning electron microscope (Fig. 2) evidence the aggregation of the mixed oxide into spherical supramolecular formations with a diameter of about 1–5 μm. These globules have a porous structure and consist of nanowires or nanoleaves, predominantly oriented from the center to the edges. It is difficult to reliably estimate the length of these fibers, and their thickness is about 15–20 nm. This value coincides with the size of the crystallites according to the results of X-ray diffraction. As can be seen in micrographs, crystallites do not exist separately, but form more massive structures. In the literature, there

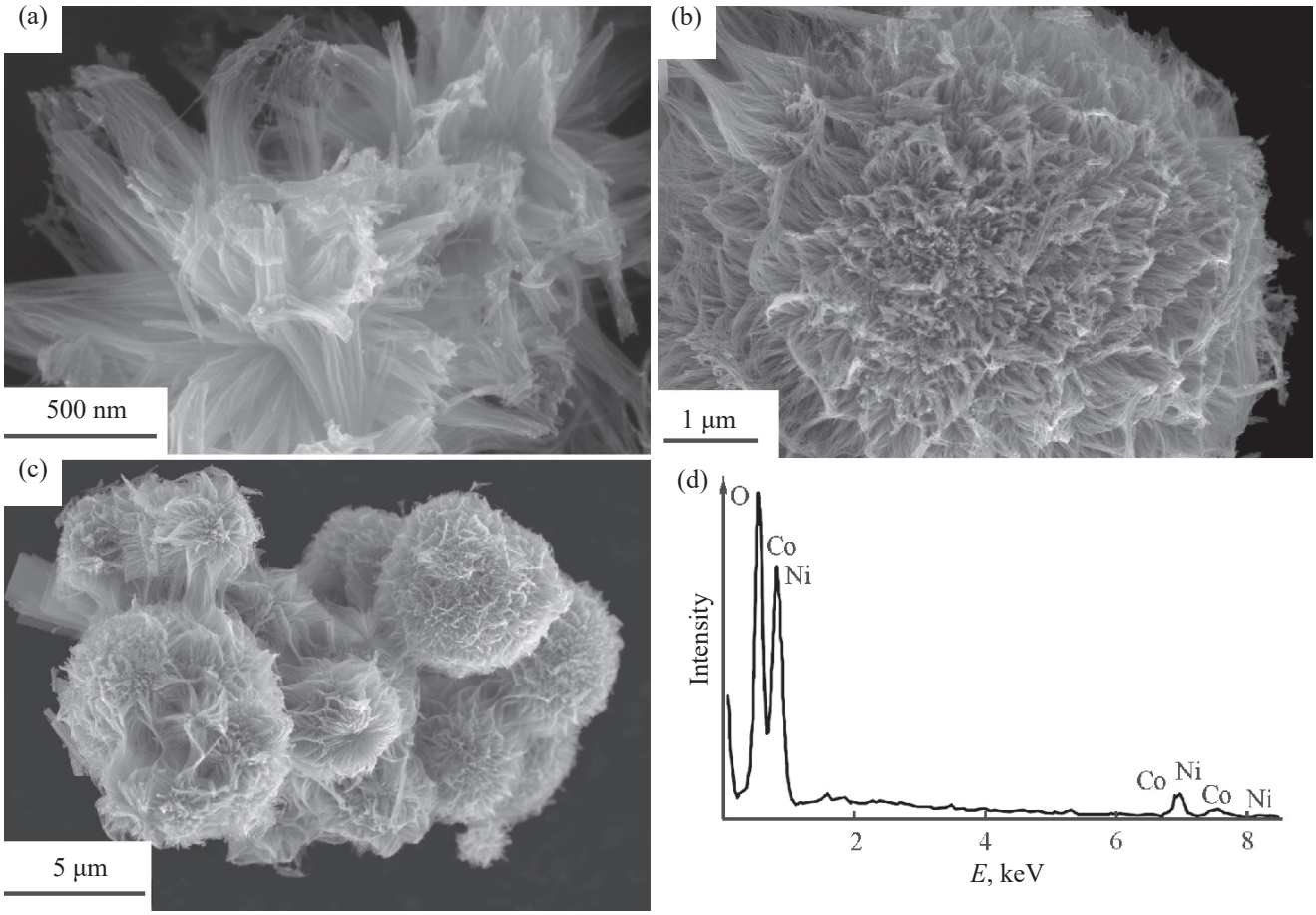

Fig. 2. Electron micrographs of (a–c) $NiCo_2O_4$ powder, energy dispersive X-ray spectrum (d) $NiCo_2O_4$ powder.

is evidence of the production by a similar method of spherical structures consisting of nanowires [24] and nanoleaves [20].

The spectrum recorded using energy dispersive X-ray spectroscopy (Fig. 2d) additionally confirms the composition of the obtained powder.

On the cyclic voltammograms of the prepared electrodes (Fig. 3), one main pair of broad redox peaks is observed. The shape of these cyclic voltammograms with pronounced current peaks is characteristic of materials of this type and indicates the occurrence of Faradaic processes corresponding to the recharge of nickel and cobalt ions in the structure of the mixed oxide. The peak-shaped cyclic voltammograms for systems with Faradaic processes, i.e., systems with pseudocapacitive charge storage, are the opposite of the almost rectangular cyclic voltammograms for systems with a double-layer charging mechanism, when there is a constant charging current of a double-layer capacity [2]. The latter is typical of traditional double-layer capacitors. Thus, the accumulation of an electric charge on such an electrode made of mixed nickel and cobalt oxide occurs due to the Faradaic pseudocapacitance associated with a change in the oxidation states of nickel (3+/2+) and cobalt (3+/2+) in the oxide film.

The potential of the anodic peak at a potential scan rate of 5 mV s^{-1} is ~0.37 V for the NC_{NMP} and NC_{foam} samples and 0.29 V for the NC_{eth} sample. The potential for the cathodic peak is 0.23, 0.22, and 0.18 V for NC_{NMP}, NC_{foam}, and NC_{eth}, respectively. The positions of the cathodic and anodic peaks, as well as the absence of their separation into individual nickel and cobalt peaks, are consistent with the data of [25, 26].

Noteworthy is the fact that at the lowest potential scan rate (5 mV s^{-1}, Fig. 3a) the potentials of the onset of the anodic (E_a = 0.31, 0.24, and 0.27 V for NC_{NMP}, NC_{eth}, and NC_{foam}, respectively) and cathodic (E_c = 0.31, 0.22, and 0.26 V for NC_{NMP}, NC_{eth}, and NC_{foam},

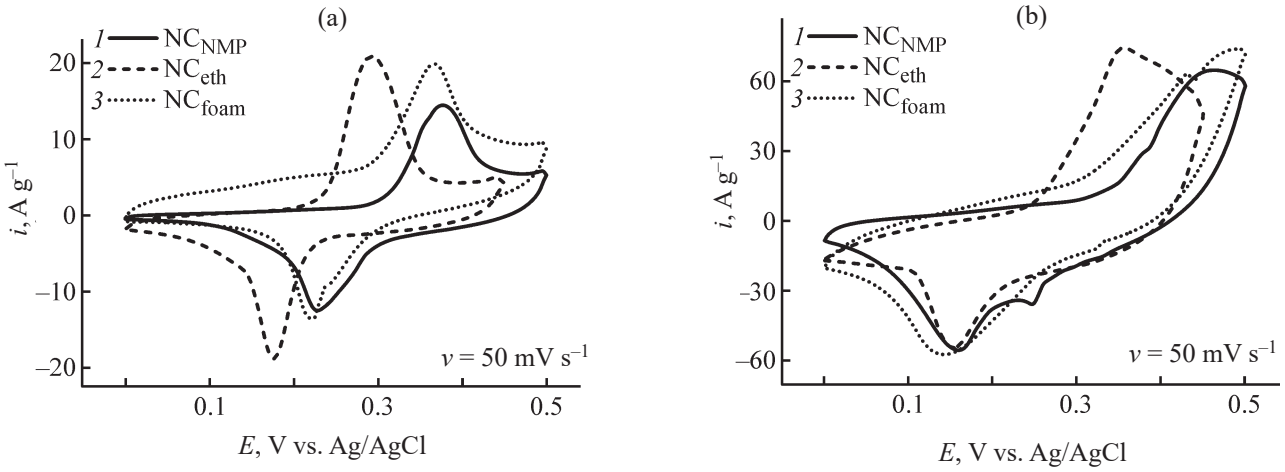

Fig. 3. Cyclic voltammograms of electrodes based on $NiCo_2O_4$ in a 2 M KOH solution that were prepared by various methods at a potential scan rate of (a) 5 and (b) 50 mV s^{-1}.

respectively) processes were quite close. This indicates that at low currents, when the potential shift due to the ohmic resistance of the material and diffusion restrictions is small, the onset of redox reactions of mixed nickel-cobalt oxide occurred at relatively close potential values.

As the potential scan rate increases, the peaks become less pronounced, which is also reported in the literature [27]. In the case of the NC_{NMP} and NC_{foam} samples, the anodic peaks at 50 mV s^{-1} [$i_{p,a}$ (NC_{NMP}) = 0.46 V, $i_{p,a}$ (NC_{foam}) = 0.49 V] are not fully resolved. The potentials of the cathodic peaks are 0.16, 0.15, and 0.14 V for NC_{NMP}, NC_{eth}, and NC_{foam}, respectively. It is noteworthy that in the case of the NC_{eth} sample, the shift of the peak potentials with an increase in the potential scan rate is minimal, which may indicate a faster recharge of the material, in contrast to other samples. The decrease in the performance of the material with an increase in the scan rate is consistent with the known literature data [28, 29].

When the cyclic voltammograms are normalized to the potential scan rate (Figs. 4a, 4c, 4e), the redox peak currents do not coincide, and the area under the peaks noticeably diminishes with an increase in the scan rate, which indicates a decrease in the redox capacity of the material. The scan rate also affects the peak potentials: with an increase in the scan rate, the cathodic and anodic peak separation rises significantly. This fact indicates an increase in the degree of irreversibility of the electrode process and an increase in the ohmic component of the shift of the peak potentials. The observed phenomena are characteristic of materials with reversible redox capacity [30].

With an increase in the potential scan rate from 5 to 200 mV s^{-1}, the anodic peaks shifted towards positive potentials. At the same time, the position of the cathode peaks changed little with an increase in the potential scan rate in the indicated range.

According to the data available in the literature, the peaks observed in cyclic voltammograms are of a complex nature and can be attributed to the redox processes of nickel and cobalt recharge in the composition of the mixed oxide by the following reactions [7, 31–35]:

$$NiCo_2O_4 + OH^- + H_2O \leftrightarrow NiOOH + 2CoOOH + e, \quad (1)$$

$$CoOOH + OH^- \leftrightarrow CoO_2 + H_2O + e, \quad (2)$$

$$NiOOH + OH^- \leftrightarrow NiO_2 + H_2O + e. \quad (3)$$

Despite the occurrence of at least three processes of nickel recharge and cobalt recharge, peak separation is not observed even when the scan rate decreases to 1 mV s^{-1} (Fig. 4c), which is consistent with the data of [27, 36, 37].

We analyzed the dependences of the anodic peak currents on the potential scan rate (Figs. 4b, 4d, 4f). In the first approximation, the same linear dependence of log $I_{p,a}$ vs. log ν is observed. The slope of the dependences of the peak currents on the scan rate (tan α) was in all studied cases within the range of 0.57–0.85, which exceeds the expected slope (0.5) for the case of a diffusion-controlled current. The increased slope of the dependence can be explained by the partial contribution

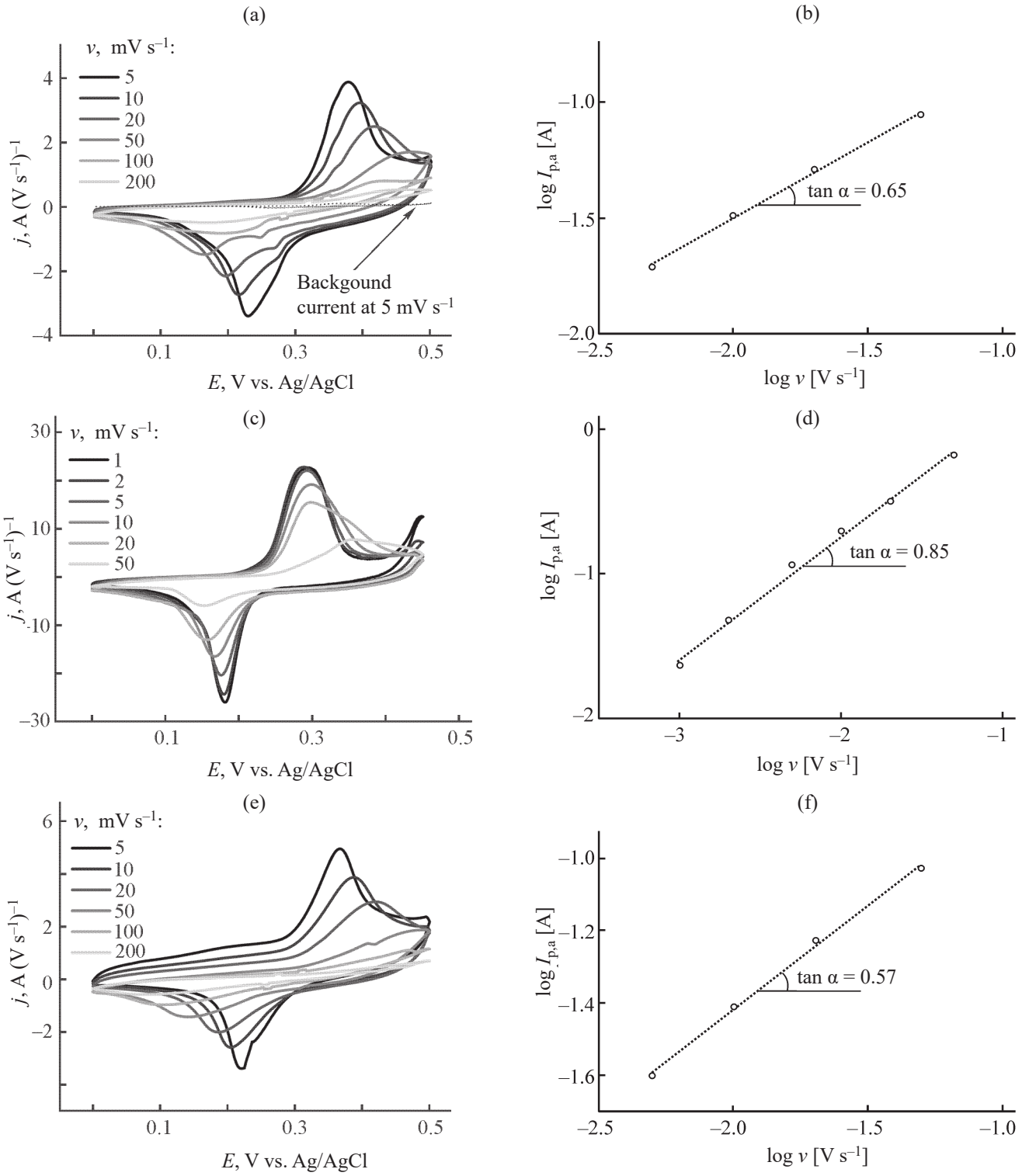

Fig. 4. (a, c, e) Cyclic voltammograms at various potential scan rates in 2 M KOH and (b, d, f) logarithmic dependences of the anode peak current on the scan rate for materials (a, b) NC_{NMP}, (c, d) NC_{eth}, and (e, f) NC_{foam}.

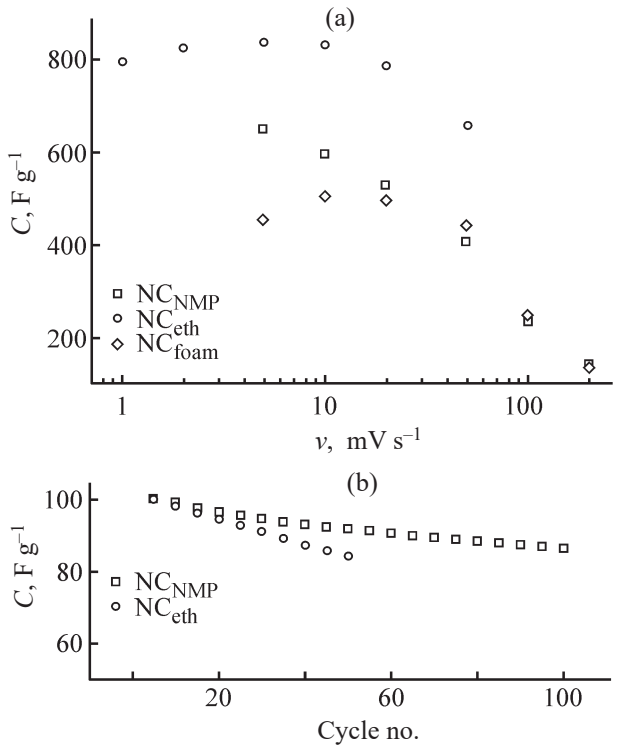

Fig. 5. Material capacity vs. (a) the potential scan rate and (b) the cycle number at $\nu = 50$ mV s^{-1}.

of the processes caused by the recharge of nickel and cobalt ions in the material composition, to the recorded currents, when a directly proportional dependence (slope tan $\alpha = 1$) should be observed for this total current component.

The specific capacity C of the prepared electrodes, normalized to the mass of the mixed oxide, was calculated by the formula

$$C = Q/(\Delta E m),$$

where Q is the amount of electricity determined by integrating the cathode region of the current–voltage curve; ΔE is potential range; m is the mass of the mixed oxide on the electrode.

The highest specific capacities for various potential scan rates are registered for the NC_{eth} material: 840 F g^{-1} at 5 mV s^{-1} and 660 F g^{-1} at 50 mV s^{-1} (Fig. 5a), which is a small decrease in capacity with increasing potential scan rate. A significant disadvantage of the material is the rapid loss of capacity (15% over 50 cycles) associated with dissolution. A similar disadvantage is also inherent in the NC_{foam} sample, but the specific capacity of this sample is initially lower: 450 and 440 F g^{-1} at 5 and 50 mV s^{-1}, respectively. The NC_{NMP} sample, which is a kind of "conventional" sample, since it was created using a polyvinylidene fluoride binder and the most common solvent *N*-methylpyrrolidone, shows average specific capacities compared to the other two samples: 650 and 410 F g^{-1} at 5 and 50 mV s^{-1}, respectively. Both samples, NC_{foam} and NC_{NMP}, demonstrate a significant drop in specific capacity with a further rise in the potential scan rate—140 F g^{-1} at 200 mV s^{-1} in both cases.

Nevertheless, the reached values of specific capacity (in particular, 840 F g^{-1} for NC_{eth}) allow considering these materials as promising for further research and use as electrodes in supercapacitors [38–40]. Another aspect of the NC_{eth} material is also noteworthy: in this case, the material mass loading is about 5 mg cm^{-2}, while other samples exhibit lower capacity values even at a low mass loading of about 1 mg cm^{-2}. The main problem to be solved for the NC_{eth} material is its low stability, probably resulting from the choice of a solvent, which, although it has good ability to penetrate into the pores of nickel foam, is only able to disperse polyvinylidene fluoride, and not dissolve it. As a result, the finished material turns out to be "unconfined" in the binder polymer structure. Thus, NC_{NMP} retains 87% of its initial capacity after 100 recharge cycles (and 92% after 50 cycles), while NC_{eth} retains 84% of its initial capacity after 50 cycles.

CONCLUSIONS

The study results allow conclusion that the capacity and stability of materials based on $NiCo_2O_4$ depend significantly on the method of mixed nickel-cobalt oxide deposition on the substrate even under the same synthesis conditions. The standard deposition method using *N*-methylpyrrolidone solvent provides relatively low capacity and results in a large capacity loss (37%) when the scan rate increases from 5 to 50 mV s^{-1}. The use of ethanol as a solvent provides a greater degree of penetration of the material into the pores of the nickel foam substrate and increases the material capacity by 30% compared to the analogue prepared with *N*-methylpyrrolidone, although the stability of the material decreases during cycling. In the case of direct synthesis of a material on a substrate, the number of steps is reduced, which is favorable for production; however, a low mass loading of a substance and low stability

require further research to improve the properties of electrodes.

ACKNOWLEDGMENTS

The studies by scanning electron microscopy, energy dispersive X-ray spectroscopy and powder X-ray diffraction were carried out using the equipment of "Interdisciplinary Resource Centre for Nanotechnology" and "Centre for X-ray Diffraction Studies" of the Research Park of St. Petersburg State University.

FUNDING

This work was carried out with the financial support of St. Petersburg State University (grant no. 26455158).

CONFLICT OF INTERESTS

The authors declare that they have no conflicts of interest requiring disclosure in this article.

REFERENCES

1. Zhang, G., Xiao, X., Li, B., Gu, P., Xue, H., and Pang, H.J., *Mater. Chem. A,* 2017, vol. 5, no. 18, pp. 8155–8186. https://doi.org/10.1039/c7ta02454a
2. Kate, R. S., Khalate, S. A., and Deokate, R.J.J., *Alloys Compd.,* 2018, vol. 734, pp. 89–111. https://doi.org/10.1016/j.jallcom.2017.10.262
3. Wang, G.P., Zhang, L., and Zhang, J.J., *Chem. Soc. Rev.,* 2012, vol. 41, no. 2, pp. 797–828. https://doi.org/10.1039/c1cs15060j
4. Adán-Más, A., Silva T. M., Guerlou-Demourgues, L., Bourgeois, L., Labrugere-Sarroste, C., and Montemor, M.F., *J. Power Sources,* 2019, vol. 419, pp. 12–26. https://doi.org/10.1016/j.jpowsour.2019.02.055
5. Wang, X., Liu W., S., Lu, X., and Lee, P.S., *J. Mater. Chem.,* 2012, vol. 22, no. 43, pp. 23114–23119. https://doi.org/10.1039/c2jm35307e
6. Dang, S., Wang, Z., Jia, W., Cao, Y., and Zhang, J., *Mater. Res. Bull.,* 2019, vol. 116, no. 1, pp. 117–125. https://doi.org/10.1016/j.materresbull.2019.04.023
7. Dubal D. P., Gomez-Romero, P., Sankapal B. R., and Holze, R., *Nano Energy,* 2015, vol. 11, pp. 377–399. https://doi.org/10.1016/j.nanoen.2014.11.013
8. Shen, L., Yu, L., Yu X. Y., Zhang, X., and Lou, X.W.D., *Angew. Chem. Int. Ed.,* 2015, vol. 54, no. 6, pp. 1868–1872. https://doi.org/10.1002/anie.201409776
9. Li, Y., Hasin, P., and Wu, Y., *Adv. Mater.,* 2010, vol. 22, no. 17, pp. 1926–1929. https://doi.org/10.1002/adma.200903896
10. Sun, B., Zhang, J., Munroe, P., Ahn, H.J., and Wang, G., *Electrochem. Commun.,* 2013, vol. 31, pp. 88–91. https://doi.org/10.1016/j.elecom.2013.03.023
11. Poonam, K., Sharma, K., Arora, A., and Tripathi, S. K., *J. Energy Storage,* 2019, vol. 21, no. 1, pp. 801–825. https://doi.org/10.1016/j.est.2019.01.010
12. Deng, F., Yu, L., Sun, M., Lin, T., Cheng, G., Lan, B., and Ye, F., *Electrochim. Acta,* 2014, vol. 133, pp. 382–390. https://doi.org/10.1016/j.electacta.2014.04.070
13. He, G., Wang, L., Chen, H., Sun, X., and Wang, X., *Mater. Lett.,* 2013, vol. 98, pp. 164–167. https://doi.org/10.1016/j.matlet.2013.02.035
14. Liu, J., Liu, C., Wan, Y., Liu, W., Ma, Z., Ji, S., Wang, J., Zhou, Y., Hodgson, P., and Li, Y., *CrystEngComm.,* 2013, vol. 15, no. 8, pp. 1578–1585. https://doi.org/10.1039/c2ce26632f
15. Wei, T.Y., Chen, C.H., Chien, H.C., Lu, S.Y., and Hu, C.C, *Adv. Mater.,* 2010, vol. 22, no. 3, pp. 347–351. https://doi.org/10.1002/adma.200902175
16. Tamilselvi, R., Padmanathan, N., Mani Rahulan, K., Mohana Priya, P., Sasikumar, R., and Mandhakini, M., *J. Mater. Sci.: Mater. Electron.,* 2018, vol. 29, no. 6, pp. 4869–4880. https://doi.org/10.1007/s10854-017-8444-7
17. Luo, Y., Zhang, H., Guo, D., Ma, J., Li, Q., Chen, L., and Wang, T., *Electrochim. Acta,* 2014, vol. 132, pp. 332–337. https://doi.org/10.1016/j.electacta.2014.03.179
18. An, Y., Hu, Z., Guo, B., An, N., Zhang, Y., Li, Z., Yang, Y., and Wu, H., *RSC Advances,* 2016, vol. 6, no. 44, pp. 37562–37573. https://doi.org/10.1039/c6ra04788b
19. Aricò, A.S., Bruce, P., Scrosati, B., Tarascon, J.M., and Van Schalkwijk, W., *Nat. Mater.,* 2005, vol. 4, no. 5, pp. 366–377. https://doi.org/10.1038/nmat1368
20. Zhang, J., Liu, F., Cheng, J. P., and Zhang, X.B., *ACS Appl. Mater. Interfaces,* 2015, vol. 7, no. 32, pp. 17630–17640. https://doi.org/10.1021/acsami.5b04463
21. Salunkhe, R.R., Jang, K., Yu, H., Yu, S., Ganesh, T., Han, S.H., and Ahn, H., *J. Alloys Compd.,* 2011, vol. 509, no. 23, pp. 6677–6682. https://doi.org/10.1016/j.jallcom.2011.03.136
22. Zeng, Z., Zhu, L., Han, E., Xiao, X., Yao, Y., and Sun, L., *Ionics,* 2019, vol. 25, no. 6, pp. 2791–2803. https://doi.org/10.1007/s11581-018-2813-y

23. Liu, C., Jiang, W., Hu, F., Wu, X., and Xue, D., *Inorg. Chem. Front,* 2018, vol. 5, no. 4, pp. 835–843. https://doi.org/10.1039/c8qi00010g

24. Zou, R., Xu, K., Wang, T., He, G., Liu, Q., Liu, X., Zhang, Z., and Hu, J., *J. Mater. Chem. A,* 2013, vol. 1, no. 30, pp. 8560–8566. https://doi.org/10.1039/c3ta11361b

25. Wu, Y.Q., Chen, X.Y., Ji, P.T., and Zhou, Q.Q., *Electrochim. Acta,* 2011, vol. 56, no. 22, pp. 7517–7522. https://doi.org/10.1016/j.electacta.2011.06.101

26. Lu, Q., Chen, Y., Li, W., Chen, J.G., Xiao, J.Q., and Jiao, F., *J. Mater. Chem. A,* 2013, vol. 1, no. 6, pp. 2331–2336. https://doi.org/10.1039/c2ta00921h.

27. Huang, L., Chen, D., Ding, Y., Feng, S., Wang, Z.L., and Liu, M., *Nano Lett.,* 2013, vol. 13, no. 7, pp. 3135–3139. https://doi.org/10.1021/nl401086t

28. Yedluri, A.K. and Kim, H.J., *RSC Advances,* 2019, vol. 9, no. 2, pp. 1115–1122. https://doi.org/10.1039/c8ra09081e

29. Wang, L., Jiao, X., Liu, P., Ouyang, Y., Xia, X., Lei, W., and Hao, Q., *Appl. Surf. Sci.,* 2018, vol. 427, pp. 174–181. https://doi.org/10.1016/j.apsusc.2017.07.221

30. Silva R. P., Eugénio, S., Duarte, R., Silva T. M., Carmezim, M. J., and Montemor, M. F., *Electrochim. Acta,* 2015, vol. 167, pp. 13–19. https://doi.org/10.1016/j.electacta.2015.03.083

31. Li, S., Yang, K., Ye, P., Jiang, H., Zhang, Z., Huang, Q., and Wang, L., *Appl. Surf. Sci.,* 2019, vol. 473, pp. 326–333. https://doi.org/10.1016/j.apsusc.2018.12.160

32. Ramesh, S., Vikraman, D., Kim, H.S., Kim, H.S., and Kim, J.H., *J. Alloys Compd.,* 2018, vol. 765, pp. 369–379. https://doi.org/10.1016/j.jallcom.2018.06.194

33. Zhu, Y., Pu, X., Song, W., Wu, Z., Zhou, Z., He, X., Lu, F., Jing, M., Tang, B., and Ji, X., *J. Alloys Compd.,* 2014, vol. 617, pp. 988–993. https://doi.org/10.1016/j.jallcom.2014.08.064

34. Xiong, W., Hu, X., Wu, X., Zeng, Y., Wang, B., He, G.H., and Zhu, Z.H., *J. Mater. Chem. A,* 2015, vol. 3, pp. 17209–17216. https://doi.org/10.1039/C5TA04201A

35. Hu, C.C. and Cheng, C.Y., *Electrochem. Solid-State Lett.,* 2002, vol. 5, pp. A43–A46. https://doi.org/10.1149/1.1448184

36. Li, Y., Pan, J., Wu, J., Yi, T., and Xie, Y., *J. Energy Chem.,* 2019, vol. 31, pp. 167–177. https://doi.org/10.1016/j.jechem.2018.06.009

37. Li, Q., Zhang, Q., Sun, J., Liu, C., Guo, J., He, B., Zhou, Z., Man, P., Li, C., Xie, L., and Yao, Y., *Adv. Sci.,* 2019, vol. 6, no. 2, pp. 1801379. https://doi.org/10.1002/advs.201801379

38. Hsu C. T. and Hu C. C., *J. Power Sources,* 2013, vol. 242, pp. 662–671. https://doi.org/10.1016/j.jpowsour.2013.05.130

39. Jiang, H., Li, C., Sun, T., and Ma, J., *Chem. Commun.,* 2012, vol. 48, no. 20, pp. 2606–2608. https://doi.org/10.1039/c2cc18079k

40. Zhang, G.Q., Wu, H.Bm, Hoster, H.E., Chan-Park, M.B., and Lou, X.W., *Energy Environ. Sci.,* 2012, vol. 5, no. 11, pp. 9453–9456. https://doi.org/10.1039/c2ee22572g